RSC Advances

PAPER

View Article Online
View Journal | View Issue

Cite this: *RSC Adv.*, 2023, **13**, 17959

Growth of 3D-TNAs@Ti-MOFs by dual titanium source strategy with enhanced photoelectrocatalytic/photoelectro-Fenton performance for degradation of tetracycline under visible light irradiation†

Ruiyu Bao,[ab] Yue Zhao,[b] Chen Chen,[ab] Mengmeng Cui,[b] Ling Yang,[b] Jianxin Xia*[ab] and Hua Li*[ab]

Visible-light-active 3D-TNAs@Ti-MOFs composite electrodes were fabricated by decorating nanoscaled Ti-based metal–organic frameworks on three-dimensional TiO_2 nanotube arrays (3D-TNAs) prepared by a facile *in situ* solvothermal method. The photoelectrocatalytic performance of electrode materials was evaluated by degradation of tetracycline (TC) under visible light irradiation. The experiment results show that Ti-MOFs nanoparticles are highly distributed on the top and side walls of TiO_2 nanotubes. The 3D-TNAs@NH_2-MIL-125 solvothermally synthesized for 30 h exhibited the best photoelectrochemical performance compared with 3D-TNAs@MIL-125 and pristine 3D-TNAs. In order to further enhance the degradation efficiency of TC by 3D-TNAs@NH_2-MIL-125, a photoelectro-Fenton (PEF) system was constructed. The influence of H_2O_2 concentration, solution pH and applied bias potential on TC degradation were explored. The results showed that when pH was 5.5, H_2O_2 concentration was 30 mM, and applied bias was 0.7 V, the degradation rate of TC was 24% higher than the pure photoelectrocatalytic degradation process. The enhanced photoelectro-Fenton performance of 3D-TNAs@NH_2-MIL-125 could be attributed to the large specific surface area, excellent light utilization, efficient interfacial charge transfer, low electron–hole recombination rate and high production of $^{\bullet}OH$ as the result of the synergistic effect between TiO_2 nanotubes and NH_2-MIL-125.

Received 9th May 2023
Accepted 17th May 2023

DOI: 10.1039/d3ra03098a

rsc.li/rsc-advances

Introduction

Antibiotics have attracted wide attention due to their harmful effects on health and the environment.[1,2] Tetracycline (TC), as one of the widely used antibiotics, is frequently detected in the aquatic environment.[3] Because of its poor biodegradability, the presence of TC in water bodies causes great threats to aquatic life and human health.[4] Therefore, it is necessary to remove them from water. It is difficult to completely remove such pollutants using traditional water treatment technologies and thus, it is of great urgency to develop advanced water treatment technologies with environmentally-friendly and high efficiency to remove refractory pollutants.[5,6] Electrochemical advanced oxidation processes (EAOPs) have been widely studied for removing recalcitrant pollutants through the generation of reactive oxygen species (ROS), which could react non-selectively with the organic pollutants, and eventually mineralize them to CO_2 and H_2O.[7,8] Among them, photoelectrocatalytic (PEC) and photoelectro-Fenton (PEF) processes have become a hot spot of research in recent years. In the PEC process, the holes (h^+) oxidize water into hydroxyl radical ($^{\bullet}OH$) in the photoanode surface, the electrons (e^-) are transferred to the cathode and reduce the oxygen to form superoxide radicals ($^{\bullet}O_2^-$). In the PEF process, hydrogen peroxide (H_2O_2) is activated on the surface of cathode and produce $^{\bullet}OH$.[7] The key to the above reaction is to find a good electrode material.

TiO_2 nanotube arrays is widely used as an electrode material due to its high stability, large specific surface area, environmental friendliness, efficient photoactivity, good recyclability and low cost.[9,10] And the nanotubular structure favors the separation of photogenerated electrons and holes.[11] In addition, the TiO_2 nanotubes grown on the mesh substrate have a three-dimensional (3D) configuration, which could provide larger active areas and enhance the light absorption capability. Therefore, TiO_2 nanotubes grown on titanium mesh showed significantly enhanced catalytic activity compared with those

[a]*Key Laboratory of Ecology and Environment in Minority Areas (Minzu University of China), National Ethnic Affairs Commission, Beijing 100081, China. E-mail: lihua@muc.edu.cn; jxxia@vip.sina.com*

[b]*College of Life and Environmental Sciences, Minzu University of China, Beijing 100081, China*

† Electronic supplementary information (ESI) available. See DOI: https://doi.org/10.1039/d3ra03098a

grown on titanium foils.[12–14] However, pristine TiO_2 nanotubes are only sensitive to the UV light due to its wide band gap, which results in low solar energy utilization.[11] In order to solve the above problems, we use the method of semiconductor coupling to extend absorption spectrum to the visible light region and improve the efficiency of electron–hole separation.[15]

Metal–organic frameworks (MOFs) constructed of metal ions (or clusters) and organic linkers have received wide attention as the photocatalysts because of their large specific surface area, easy surface functionalization and abundant active sites.[4,16–18] Among them, the titanium-based MOF (MIL-125 or NH_2-MIL-125) has excellent properties such as non-toxicity, high density of Ti sites and high chemical stability.[18] In particular, amino-functionalized Ti-based MOFs shows a good response to visible light.[15] In addition, due to TiO_2 is a homologous metal oxide of Ti-MOFs, it can increase the heterogeneous nucleation sites during formation of Ti-MOFs. Therefore, the combination of TiO_2 nanotubes and NH_2-MIL-125 to form composite materials is an effective way to enhance the visible-light catalytic activity. Xue *et al.* synthesized TiO_2 nanotube arrays decorated by MIL-125 or NH_2-MIL-125 using solvothermal method, exhibiting a high photocatalytic activity.[11] Song *et al.* prepared TiO_2 nanotubes decorated by NH_2-MIL-125 (Ti) using hydrothermal method, which has high photoelectrocatalytic hydrogen production activity. The hydrogen production rate was 14 times higher than that of the pristine TiO_2 nanotubes as a photoanode.[17]

Herein, we report that three-dimensional TiO_2 nanotube arrays (3D-TNAs) decorated by MIL-125 or NH_2-MIL-125 particles (named 3D-TNAs@MIL-125 and 3D-TNAs@NH_2-MIL-125) were fabricated by *in situ* solvothermal method. Detailed photoelectrochemical characterizations indicate that 3D-TNAs@NH_2-MIL-125 composite electrode shows excellent photoelectrochemical performance compared with 3D-TNAs@MIL-125 and pristine 3D-TNAs. Meanwhile, we constructed a photoelectro-Fenton (PEF) system to further enhance the degradation efficiency of TC with 3D-TNAs@NH_2-MIL-125 as anode and cathode. The effect of H_2O_2 concentration, solution pH and applied bias potential on TC removal were explored. The possible mechanism for the enhanced catalytic performance was discussed.

Materials and methods

Materials

Titanium meshes (100 mesh per inch; purity 99.95%) were purchased from Hebei Anping Dakewei Metal Wire Mesh Products Limited Co. China. *N*,*N*-Dimethylformamide (DMF), methanol (CH_3OH), terephthalic acid (H_2BDC), 2-amino-terephthalic acid (NH_2–H_2BDC), titanium tetraisopropanolate (TTiP), tetracycline (TC), isopropanol (IPA), triethanolamine (TEOA) and hydrogen peroxide (30 wt% H_2O_2) were analytical grade purity purchased from Sinopharm Group Co., and used without further purification. Ultrapure water (Milli-Q $\rho = 18.2$ MΩ cm/25 °C) was used throughout this study.

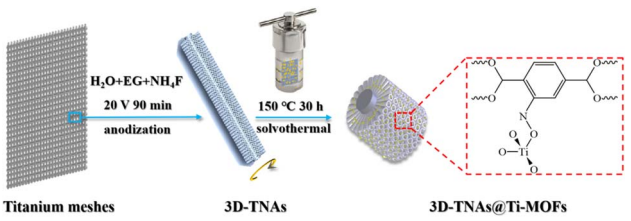

Fig. 1 Schematic illustration of the preparation route of 3D-TNAs@Ti-MOFs.

Synthesis of 3D-TNAs@Ti-MOFs composite electrodes

The 3D-TNAs were synthesized by anodization in fluorinated ethylene glycol, which is consistent with previous report.[12] 3D-TNAs@Ti-MOFs composite electrodes were synthesized by an *in situ* solvothermal method. The synthetic process of 3D-TNAs@Ti-MOFs is shown in Fig. 1. Firstly, NH_2–H_2BDC (3 mmol) and TTiP (1 mmol) were added in a mixture of DMF and CH_3OH (with volume ratios of DMF : CH_3OH = 9 : 1)[15] under stirring for 30 min at room temperature. Then, the above solution was transferred to a 50 mL Teflon-lined stainless-steel autoclave. Then the 3D-TNAs were immersed in the solution and heated at 150 °C for different times (20, 25, 30, 35 and 40 h). Afterward, the 3D-TNAs@NH_2-MIL-125 composite electrodes were obtained by washing with DMF and CH_3OH for three times. Finally the 3D-TNAs@NH_2-MIL-125 was dried at 60 °C in the vacuum oven. The powders in the autoclave were also collected by centrifugation, washing and vacuum drying at 60 °C. 3D-TNAs@MIL-125 was synthesized under the same conditions except H_2BDC as ligand.

Characterization

The surface morphology of Ti-MOFs, 3D-TNAs and 3D-TNAs@Ti-MOFs electrodes were characterized by scanning electron microscopy (SEM, Hitachi s-4800). The crystal structure of Ti-MOFs, 3D-TNAs and 3D-TNAs@Ti-MOFs electrodes were characterized using XD-3 X-Ray Diffractometer (XRD) with a Cu target (K_α radiation, $\lambda = 1.5406$ Å). Light absorption property of Ti-MOFs, 3D-TNAs and 3D-TNAs@Ti-MOFs electrodes were measured by UV-vis diffuse reflectance spectroscopy (DRS, Lambda 950).

Photocurrent test

Photoelectrochemical measurements were performed on a three-electrode electrochemical workstation (CHI 660E, Chenhua, China) using three-dimensional electrode as the working electrode, a platinum foil as the counter electrode and Ag/AgCl electrode as the reference electrode. A 0.1 M Na_2SO_4 solution containing 25% methanol was used as electrolyte. The visible light source was obtained by the Xe lamp (PLS-SXE 300/300UV) with 420 nm cut-off filter. Photocurrents were obtained from *i*–*t* measurements.

Degradation tests

The degradation of TC was used to evaluate the photoelectrocatalytic performance of electrode materials. A quartz photochemical reactor was used in photoelectrochemical tests with 10 mg L^{-1} TC solutions containing 0.1 M Na_2SO_4. The

reaction temperature was kept constant by cooling water circulation system. The TC solution was magnetic stirred under dark conditions for 30 min to attain an adsorption/desorption equilibrium between the photoelectrodes and TC. The initial pH value of the solution was adjusted by HCl or NaOH. A Xe lamp with 420 nm cut-off filter was used as the visible light source. A DC power (DH1766-1) supplied electricity. 4 mL solution was extracted at different irradiation times and analyzed by a UV-vis spectrophotometer (TU-1901, China) at the characteristic absorption wavelength of TC (λ_{TC} = 357 nm) to determine the extent of degradation. For the range of concentrations studied, the relationship between concentration and absorbance of TC follows the Beer–Lambert Law.

Results and discussion

Photocurrent test

The transient photocurrent was measured using a 30 s on–off visible-light irradiation cycle at a 0 V bias *vs.* Ag/AgCl electrode, and the results are shown in Fig. 2. The photocurrent value is nearly zero in dark conditions. The photocurrent appeared rapidly when the light switch turned on. As shown in Fig. 2a, the photocurrent of 3D-TNAs@Ti-MOFs starts to spike and then tends to a steady state. The photocurrent densities of 3D-TNAs@Ti-MOFs were significantly higher than that of 3D-TNAs (0.02 mA cm^{-2}). Among them, 3D-TNAs@NH_2-MIL-125 showed the highest photocurrent response under visible light irradiation, indicating that it has a lower electron–hole recombination rate and better photoelectrochemical performance. Fig. 2b shows the transient photocurrent densities of 3D-TNAs@NH_2-MIL-125 at different solvothermal synthesis times. The 3D-TNAs@NH_2-MIL-125 solvothermally synthesized for 30 h exhibited the highest photocurrent density, indicating that the optimal reaction conditions for solvothermal synthesis are 150 °C for 30 h. Therefore, this electrode material was selected for subsequent experiments.

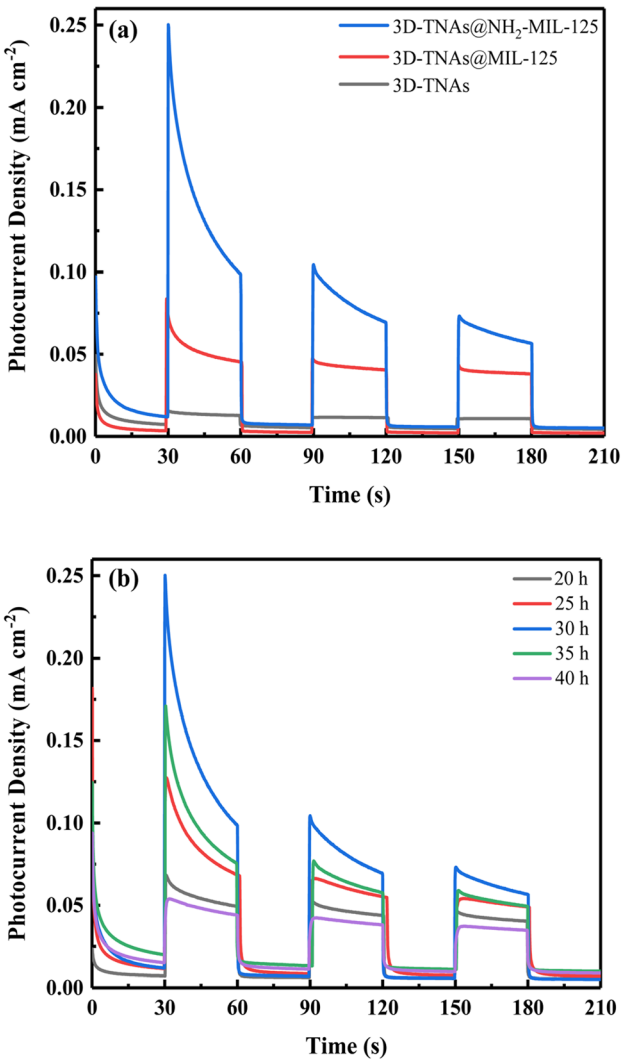

Fig. 2 (a) *i*–*t* characteristics of 3D-TNAs, 3D-TNAs@MIL-125 and 3D-TNAs@NH_2-MIL-125 as working electrodes under visible light irradiation. (b) *i*–*t* characteristics of 3D-TNAs@NH_2-MIL-125 with different synthesis times under visible light irradiation.

Surface morphology

Fig. 3a, S1a and b† show the surface morphology of 3D-TNAs under varied magnifications. TiO_2 nanotubes were grown around each Ti wire to form 3D configuration and exhibited highly ordered nanotubular structure (Fig. S1a and b†). As shown in Fig. 3a, the average inner diameter of the TiO_2 nanotubes are 40 nm. Fig. 3b–d show the SEM images of 3D-TNAs@NH_2-MIL-125 prepared using an *in situ* solvothermal method for 30 h. From the cross-section image (Fig. 3b), the NH_2-MIL-125 nanoparticles are distributed on the top and side wall of TiO_2 nanotubes. The average particle size of NH_2-MIL-125 was about 20 nm and some of particles blocked the nozzle of TiO_2 nanotubes due to agglomeration (Fig. 3b–d). Fig. S1c† shows the SEM images of 3D-TNAs@NH_2-MIL-125 with a reaction time of 20 h. It can be seen that the loading amount and particle size of NH_2-MIL-125 are both less than those with a reaction time of 30 h, indicating that the properties of electrode materials can be tuned by solvothermal reaction time.[11] Fig. 3e–f show the SEM images of 3D-TNAs@MIL-125. A clear tubular structure can be seen, and the MIL-125 nanoparticles (~20 nm) are distributed on the top and side wall of the nanotubes. Fig. S2a and S2b† show the SEM images of the powder particles of MIL-125 and NH_2-MIL-125, respectively. The particles are ployhedron with truncated pyramid shape.[15,16] And the size of the powder particles is in the micron-level. Different from the morphology and size of powder particles, Ti-MOFs in the electrode materials become nanoscale spherical structures, which may be due to the confined space of TiO_2 nanotubes that restricts the growth of particles. Small particle size means large specific surface area, which facilitates the contact between pollutants and catalyst in the reaction process.

Crystal structure

The XRD patterns were collected from MIL-125, NH_2-MIL-125, 3D-TNAs and 3D-TNAs@Ti-MOFs electrodes, and the results are shown in Fig. 4a and b. For Ti-MOFs, the characteristic peaks at

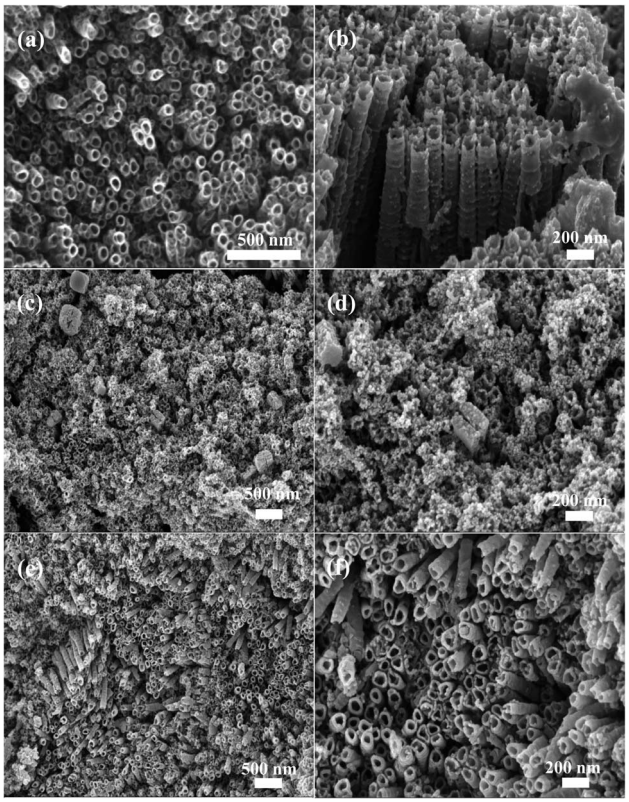

Fig. 3 SEM images of (a) unmodified 3D-TNAs on titanium mesh; (b–d) the 3D-TNAs@NH_2-MIL-125 and (e and f) 3D-TNAs@MIL-125 composite electrodes.

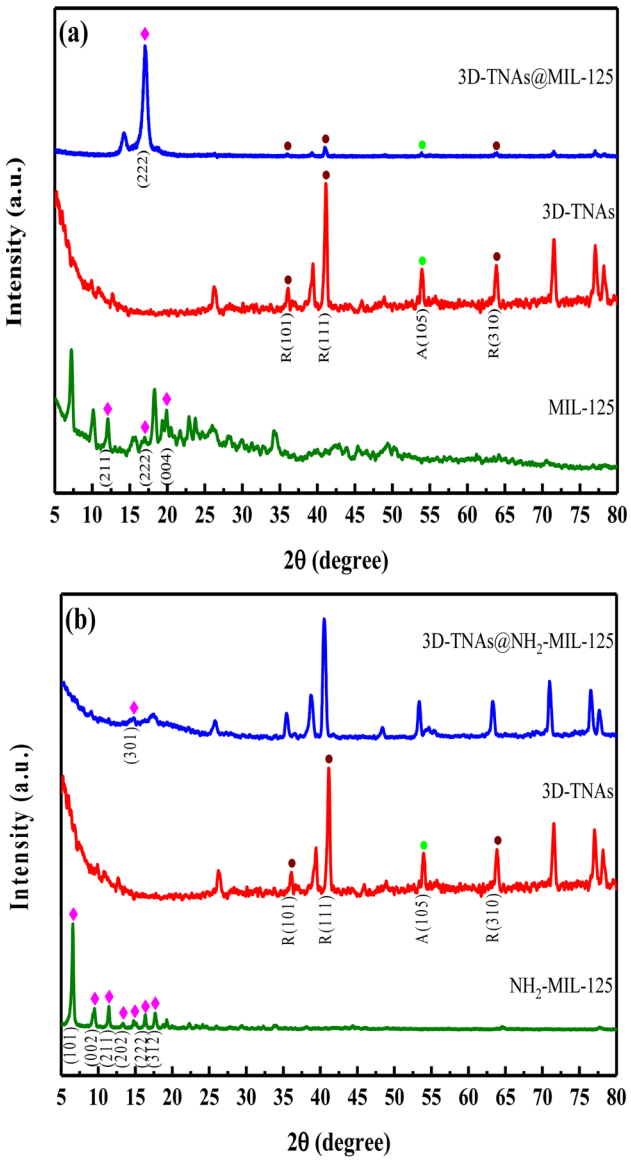

Fig. 4 XRD patterns of (a) 3D-TNAs@MIL-125, 3D-TNAs, MIL-125 and (b) 3D-TNAs@NH_2-MIL-125, 3D-TNAs, NH_2-MIL-125.

2θ values 6.7°, 9.5°, 11.5°, 13.5°, 14.9°, 16.5°, 17.7° and 19.9° can be indexed to the (101), (002), (211), (202), (301), (222), (312) and (004) planes respectively, indicating that Ti-MOFs was successfully synthesized.[19–21] For 3D-TNAs, the diffraction peak at 53.97° is corresponding to the anatase (105) phase. The diffraction peaks at 36.1°, 41.2° and 64.0° are corresponding to the rutile (101), (111) and (310) phase respectively, indicating that the synthesized electrode material is a mixture of anatase and rutile. For 3D-TNAs@Ti-MOFs, the diffraction peaks contain characteristic peaks of Ti-MOFs and TiO_2, indicating that the composite electrodes were successfully synthesized. And the diffraction peaks of 3D-TNAs@NH_2-MIL-125 are slightly shifted to the left. In addition, the characteristic peaks of Ti-MOFs encapsulate onto 3D-TNAs are weak and few, which may be due to the small particle size or low loading of Ti-MOFs on 3D-TNAs.

UV-vis spectra

Fig. S3a† shows the optical absorption properties of NH_2-MIL-125 and electrode materials. It can be seen that the absorption edge of 3D-TNAs is approximately 400 nm, indicating that the TiO_2 nanotubes mainly absorb UV light.[15] However, the 3D-TNAs@NH_2-MIL-125 composite electrode exhibits obvious absorption in the visible light region, which can generate more electron–hole pairs. In addition, NH_2-MIL-125 exhibited two absorption edges at 364 nm and 488 nm, which correspond to the absorption of Ti–O clusters and functional amine, respectively.[22,23]

The band gap energies (E_g) can be obtained by the Tauc plot. As shown in Fig. S3b,† the calculated band gap of 3D-TNAs is 3.25 eV, which is basically consistent with the reported literature.[17] The band gap of NH_2-MIL-125 is calculated to be 2.71 eV. The narrower band gap of NH_2-MIL-125 is due to the amine group serving as a chromophore.[24] Moreover, the band gap of 3D-TNAs@NH_2-MIL-125 is calculated to be 2.14 eV. The calculation result shows that the 3D-TNAs@NH_2-MIL-125 composite electrode could be excited by visible light due to the narrow band gap.

Photoelectrocatalytic activity

The photoelectrocatalytic performance of photoelectrodes were tested by the degradation of TC solution under visible light irradiation. As shown in Fig. 5a, the removal rate of TC was 33%, 50% and 64% by 3D-TNAs, 3D-TNAs@MIL-125 and 3D-

TNAs@NH_2-MIL-125 for 60 min, respectively. The 3D-TNAs@Ti-MOFs exhibited better removal efficiency comparing with 3D-TNAs. The 3D-TNAs@NH_2-MIL-125 exhibits the best photoelectrocatalytic performance, due to the narrow band-gap and efficient interfacial charge transfer between NH_2-MIL-125 and TiO_2 nanotubes.[25] The photoelectrocatalytic degradation of TC followed a pseudo-first-order reaction kinetic. Thus, the degradation rate could be characterized by the first-order kinetic constant (k) with the equation $\ln(C_0/C_t) = kt$, where C_0 was the initial concentration, C_t was the concentration of TC at time t. As shown in Fig. 5b, the kinetic constant of 3D-TNAs@NH_2-MIL-125 was 0.013 min^{-1}, which was about 2 times and 3 times of 3D-TNAs@MIL-125 (0.008 min^{-1}) and 3D-TNAs (0.005 min^{-1}), respectively. It is apparent that NH_2-MIL-125 modified TiO_2 nanotubes exhibited the optimal photoelectrochemical performance under visible light irradiation.

The effect of solution pH and applied bias potential on TC degradation by 3D-TNAs@NH_2-MIL-125 was investigated, as shown in Fig. 5c and d. When pH value increased from 3.0 to 9.0, TC removal efficiency increased from 29% to 64% after 60 min of visible light irradiation. When pH was adjusted to 12.0, the removal efficiency of TC was only 34%, which may be due to electrostatic repulsion between TC and 3D-TNAs@NH_2-MIL-125 electrode. The above results show that pH has a significant effect on photoelectrocatalytic TC degradation and alkaline solution system was beneficial to this process. Moreover, in the photocatalytic process, a small bias voltage can effectively promote the separation of photogenerated electrons and holes. In the experiment, 3D-TNAs@NH_2-MIL-125 was used as anode and platinum foil as cathode. As shown in Fig. 5d, the removal efficiency of TC increased from 57% to 64% when the applied voltage increased from 0.5 V to 0.7 V. However, the removal efficiency decreased to 49% when the applied voltage increased to 0.9 V. The thickness of the photoanode is finite, the maximum space charge layer thickness cannot exceed the semiconductor oxide films thickness. Moreover, the number of photogenerated electrons is certain at a fixed light intensity. Therefore, the saturation photocurrent is formed when the applied voltage reaches a certain value. On the contrary, as the voltage increases, side reactions will decrease the photocatalytic efficiency.[26] The above results show that the appropriate applied voltage can enhance the photoelectrocatalytic activity of electrode.[10,27] In this system, the optimal applied voltage was 0.7 V.

Fig. 6 shows the stability of 3D-TNAs@NH_2-MIL-125 under visible light irradiation. The photoelectrocatalytic efficiency of 3D-TNAs@NH_2-MIL-125 decreased by 10% after four cycles may be due to nanoparticles shedding, indicating that the 3D-TNAs@NH_2-MIL-125 photoelectrode has relatively good stability and reusability.

TC removal in PEF system

To further enhance the degradation efficiency of TC under visible light irradiation, photoelectro-Fenton (PEF) system was

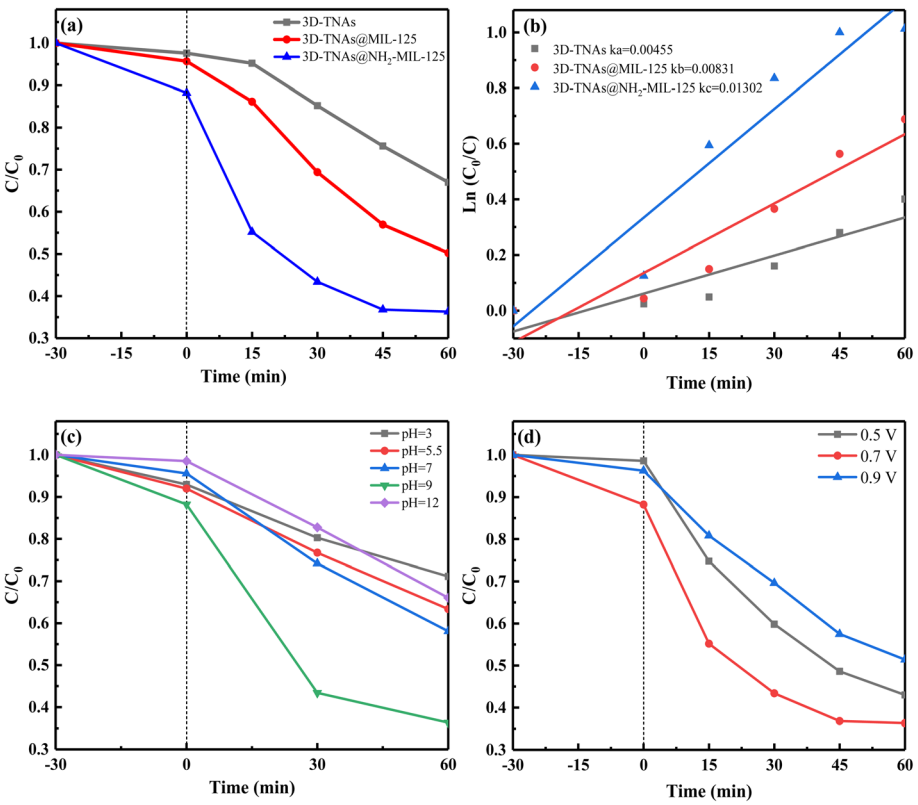

Fig. 5 (a) Photoelectrocatalytic degradation of TC with a 0.7 V bias under visible-light irradiation. (b) Photoelectrocatalytic decomposition first order kinetics profiles of TC. (c) Effect of pH on TC degradation by 3D-TNAs@NH_2-MIL-125. (d) Effect of applied bias potential on TC degradation by 3D-TNAs@NH_2-MIL-125. Conditions: TC = 10 mg L^{-1} 50 mL, pH = 9, voltage = 0.7 V, visible light ($\lambda \geq 420$ nm).

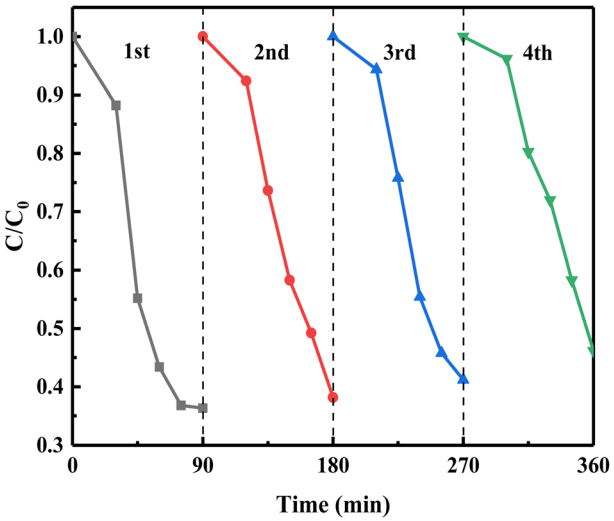

Fig. 6 Re-usability test for photoelectrocatalytic degradation of TC by 3D-TNAs@NH_2-MIL-125.

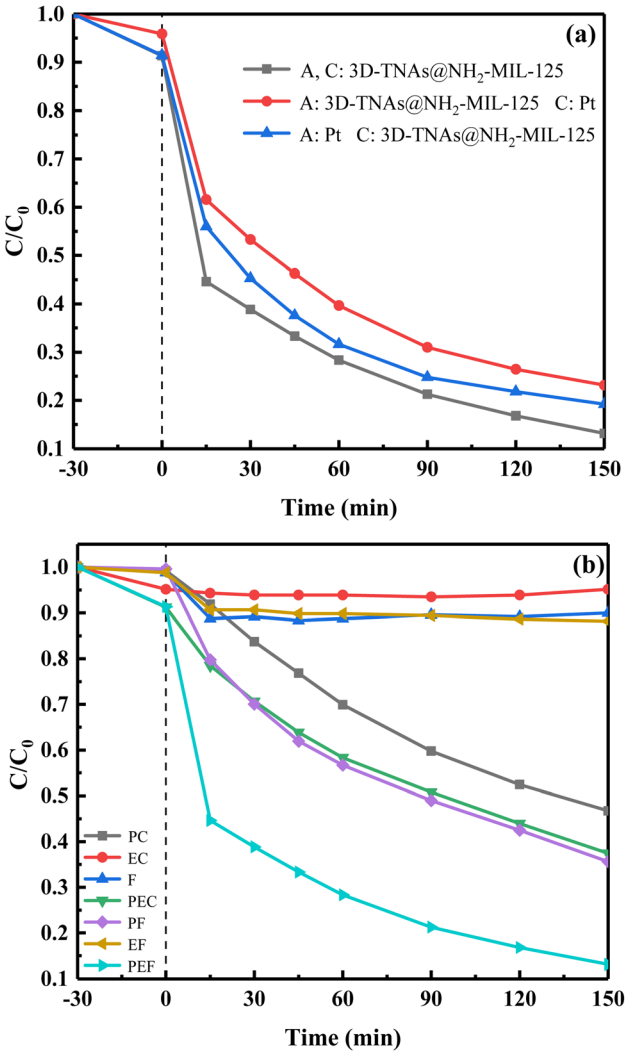

Fig. 7 (a) Photoelectro-Fenton degradation of TC with a 0.7 V bias under visible-light irradiation. (b) Degradation of TC with 3D-TNAs@NH_2-MIL-125 as a anode and cathode in different systems. Conditions: TC = 10 mg L^{-1} 200 mL, H_2O_2 = 30 mM, pH = 5.5, voltage = 0.7 V, visible light ($\lambda \geq 420$ nm).

constructed. As shown in Fig. 7a, when platinum foil was used as cathode, the removal efficiency of TC was 77%. When 3D-TNAs@NH_2-MIL-125 was used as cathode, the removal efficiency of TC was 81%. However, when 3D-TNAs@NH_2-MIL-125 was used as both anode and cathode, the removal efficiency of TC was 87%, which indicates that the catalytic performance of cathode materials determine the oxidation capacity of PEF process. Fig. 7b shows the degradation efficiency of TC under different systems, where 3D-TNAs@NH_2-MIL-125 was used as anode and cathode. As shown in Fig. 7b, TC can not be degraded in the electrocatalytic (EC) process. The degradation rate was only about 10% for the Fenton (F) and electro-Fenton (EF) system after 150 min. 53% of TC was degradation by photocatalysis (PC). As for the photoelectrocatalytic (PEC) and photo-Fenton (PF) systems, about 63% of TC was removed. However, the degradation rate was significantly increased by PEF process under visible light irradiation, which was higher than the sum of the individual processes of photoelectrocatalysis and electro-Fenton. The synergistic effect could improve the degradation of pollutants. The enhanced performance could be attributed to the higher production of $^{\bullet}OH$.[7,28]

The effect of H_2O_2 concentration, solution pH and applied bias potential on TC degradation by PEF process was studied. As shown in Fig. 8a, when the H_2O_2 concentration was zero, the removal efficiency of TC was 63%. When the concentration of H_2O_2 increases to 30 mM, the removal efficiency of TC reached the maximum (87%). However, as the concentration of H_2O_2 continues to increase, the degradation rate decreased, which is due to the fact that side reaction reduces the availability of $^{\bullet}OH$ (eqn (1)).[3,5] As shown in Fig. 8b, about 87% of TC was removed under acid conditions (pH = 3 or pH = 5.5), which was higher than that at pH 7 (72%) and pH 9 (63%). Acidic solution system was beneficial to the degradation of TC, which is due to the fact that there are enough hydrogen ions to generate H_2O_2 and further produce a large number of $^{\bullet}OH$.[29,30] Thus, the optimal pH in this system was 5.5. As shown in Fig. 8c, when the applied voltage is 0.7 V, the removal efficiency of TC was 87%. The degradation rate was about 65% when the applied voltage was 0.5 V or 0.9 V. Thus, the optimal applied voltage was 0.7 V.

$$H_2O_2 + {}^{\bullet}OH \rightarrow H_2O + {}^{\bullet}HO_2 \quad (1)$$

Mechanism analysis

The hole and free radical trapping experiments were carried out to explore the main reactive species involved in the degradation of TC. The IPA, TEOA and N_2 were used as scavengers for hydroxyl radical ($^{\bullet}OH$), holes (h^+) and superoxide radicals ($^{\bullet}O_2^-$), respectively. As shown in Fig. 9a, TEOA had the greatest effect on the degradation efficiency of TC. The degradation rate was reduced to 8%, indicating that h^+ is the main reactive species in the photoelectrocatalytic degradation of TC, followed by $^{\bullet}O_2^-$.

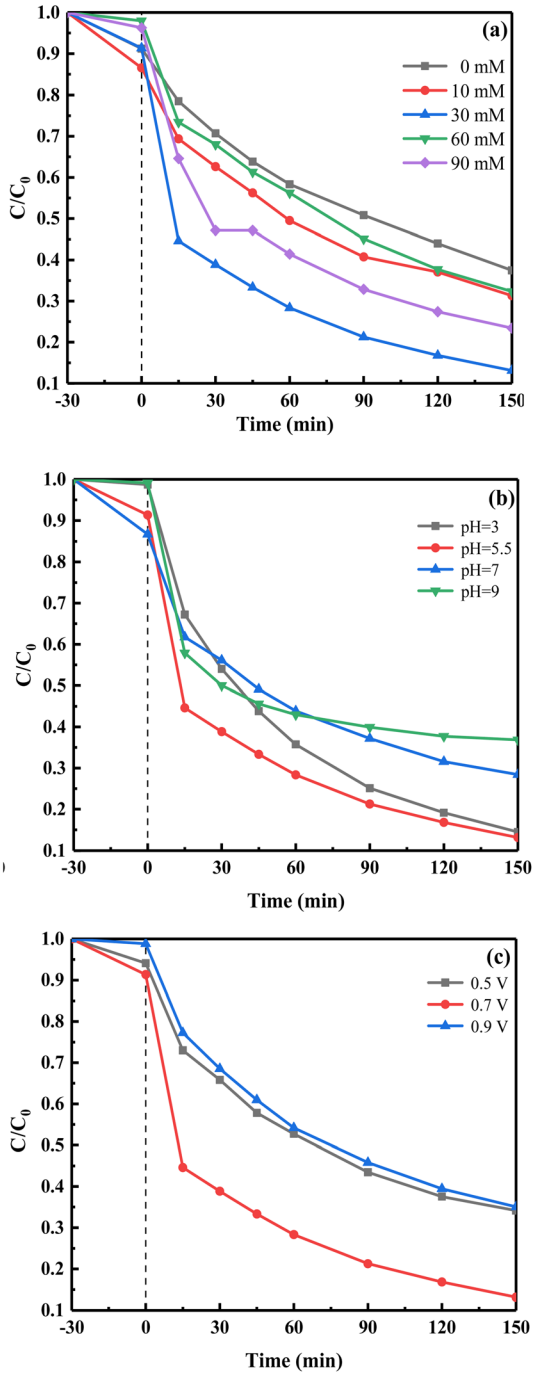

Fig. 8 Effect of (a) H_2O_2 concentration, (b) pH and (c) applied bias potential on TC removal with 3D-TNAs@NH_2-MIL-125 as a anode and cathode. Conditions: TC = 10 mg L^{-1} 200 mL, H_2O_2 = 30 mM, pH = 5.5, voltage = 0.7 V, visible light ($\lambda \geq 420$ nm).

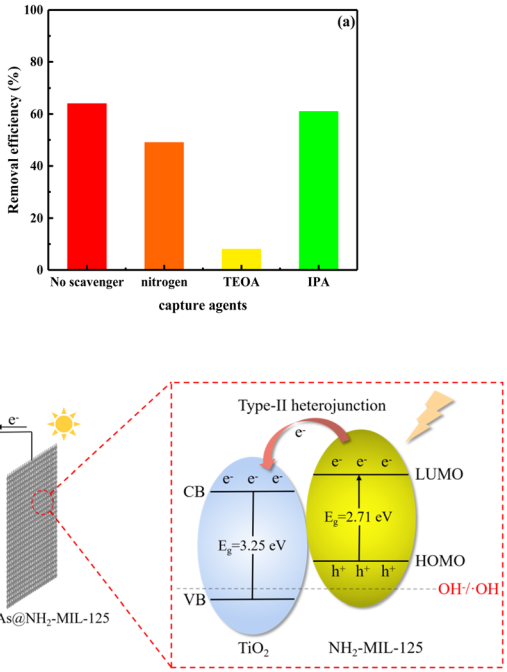

Fig. 9 (a) Effect of different scavengers on the photoelectrocatalytic removal of TC over 3D-TNAs@NH_2-MIL-125. (b) Type-II mechanism of 3D-TNAs@NH_2-MIL-125.

·OH had little effect on the degradation of TC, indicating that no ·OH was produced in PEC system. This is because the holes (h^+) in the highest occupied molecular orbital (HOMO) of NH_2-MIL-125 are not enough to oxidize OH^- to produce ·OH (Fig. 9b).

As shown in Fig. 10a, the degradation rate of TC reduced from 87% to 56% when IPA was added, indicating that ·OH is the main reactive species in PEF process, which is different from PEC process.

Moreover, the removal efficiency of TC decreased to 69% with N_2 purging, indicating that $\cdot O_2^-$ also played a role in PEF process, followed by h^+ (81%). Based on the above experimental results, we propose a possible mechanism for the enhanced degradation of TC over 3D-TNAs@NH_2-MIL-125 composite electrode, as shown in Fig. 10b. First, the TiO_2 nanotubes were grown around Ti wires to form a 3D configuration, which have a large specific surface area. Meanwhile, NH_2-MIL-125 also has a large specific surface area because of its specific 3D structure, thus the composite electrode can provide more catalytic active sites.[4,11,31] Second, the light absorption range of the composite electrode was extended to the visible region due to the functional modification of amino group.[20,21] Therefore, the catalytic activity of the electrode was improved under visible light. Third, the synergistic effect of TiO_2 and NH_2-MIL-125 is another factor for high photoelectrochemical activity. Under visible light irradiation, electrons (e^-) can be excited and transferred from the organic linkers to the titanium-oxo clusters (ligand-to-metal charge transfer, LMCT) forming Ti^{3+}.[18,22,23,32] The h^+ was left in the HOMO (eqn (2)). The e^- donated by Ti^{3+} could be transferred from the lowest unoccupied molecular orbital (LUMO) of NH_2-MIL-125 to the conduction band (CB) of TiO_2, the Ti^{3+} recovered back to Ti^{4+}.[22,23] The type-II heterojunction structure can promote the separation efficiency of the photo-generated carriers.[33] Fourth, the e^- can be transferred to the cathode through the external circuit, which could enhance the radical production.[34] The e^- could be captured by O_2 to form $\cdot O_2^-$ (eqn (3)) and H_2O_2 (eqn (4)). Meanwhile, the Ti^{4+} in NH_2-MIL-125 gains an electron to form Ti^{3+} (eqn (5)). Subsequently, the Ti^{3+} could activate H_2O_2 to produce ·OH by EF-like reaction and Ti^{3+}

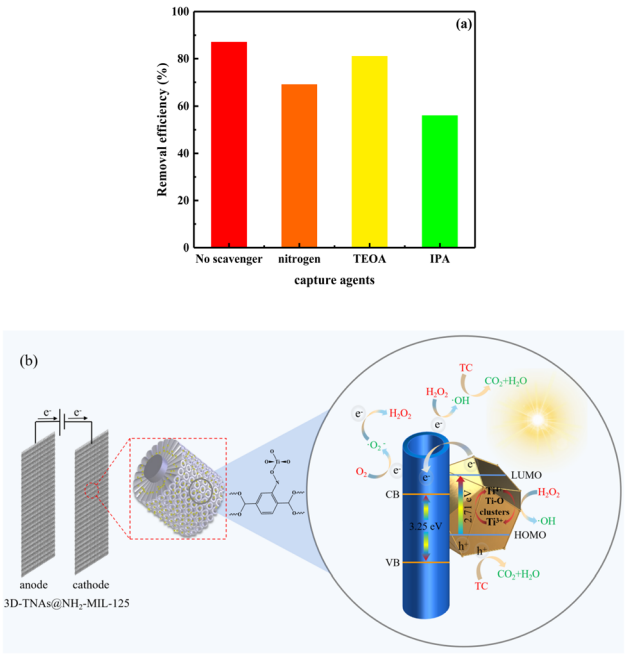

Fig. 10 (a) Effect of different scavengers on the photoelectro-Fenton removal of TC over 3D-TNAs@NH_2-MIL-125. (b) Schematic diagram of PEF degradation mechanism by 3D-TNAs@NH_2-MIL-125 under visible light irradiation.

could be oxidized to Ti^{4+} (eqn (6)), which promotes the production of ˙OH through Ti^{4+}/Ti^{3+} cycling reactions.[35] In addition, the e^- could also react with H_2O_2 to produce ˙OH (eqn (7)). And the H_2O_2 could be directly decomposed by photo energy to produce ˙OH (eqn (8)).[36] These highly reactive species can react rapidly with pollutants to achieve high photoelectrochemical performance.

$$\text{3D-TNAs@NH}_2\text{-MIL-125} + h\nu \rightarrow h^+ + e^- \quad (2)$$

$$O_2 + e^- \rightarrow {}^{\cdot}O_2^- \quad (3)$$

$$O_2 + 2H^+ + 2e^- \rightarrow H_2O_2 \quad (4)$$

$$Ti^{4+} + e^- \rightarrow Ti^{3+} \quad (5)$$

$$H_2O_2 + Ti^{3+} + H^+ \rightarrow {}^{\cdot}OH + Ti^{4+} + H_2O \quad (6)$$

$$H_2O_2 + e^- \rightarrow {}^{\cdot}OH + OH^- \quad (7)$$

$$H_2O_2 + h\nu \rightarrow 2{}^{\cdot}OH \quad (8)$$

Conclusions

In summary, the 3D-TNAs@Ti-MOFs photoelectrodes were successfully synthesized *via* anodization, followed by a facile *in situ* solvothermal method. The 3D-TNAs@NH_2-MIL-125 composite electrode shows enhanced visible light photoelectrochemical activity comparing to 3D-TNAs@MIL-125 and pristine 3D-TNAs. The photoelectro-Fenton exhibits superior TC degradation efficiency due to the higher production of ˙OH, different influence factors on degradation efficiency including H_2O_2 concentration, solution pH and applied bias potential were investigated. Under 150 min visible light irradiation, 87% of TC was degraded by 3D-TNAs@NH_2-MIL-125 in the PEF system, which was 24% higher than pure PEC degradation process. The excellent photoelectrochemical performance is attributed to the synergistic effect of TiO_2 nanotubes and NH_2-MIL-125, which can inhibit the recombination of photogenerated carriers and extend the light response to the visible region. Moreover, 3D-TNAs@NH_2-MIL-125 photoelectrodes showed good reusability and stability, indicating that it is a good candidate for applications in water purification.

Conflicts of interest

There are no conflicts to declare.

Acknowledgements

This research was funded by Key Laboratory of Ecology and Environment in Minority Areas (Minzu University of China), National Ethnic Affairs Commission [No. KLEEMA202104] and the Fundamental Research Funds for the Central Universities [No. 2022QNYL25].

Notes and references

1 Q. Zhang, G. Ying, C. Pan, *et al.*, *Environ. Sci. Technol.*, 2015, **49**(11), 6772–6782.
2 J. Shi, Y. Dong, Y. Shi, *et al.*, *Environ. Res.*, 2022, **210**, 112855.
3 Y. Yang, X. Zhang, Q. Chen, *et al.*, *ACS Omega*, 2018, **3**, 15870–15878.
4 D. Wang, F. Jia, H. Wang, *et al.*, *J. Colloid Interface Sci.*, 2018, **519**, 273–284.
5 Q. Wu, H. Yang, L. Kang, *et al.*, *Appl. Catal., B*, 2020, **263**, 118282.
6 Y. Dai, M. Liu, J. Li, *et al.*, *Sep. Sci. Technol.*, 2020, **55**, 1005–1021.
7 A. Babuponnusami and K. Muthukumar, *Environ. Sci. Pollut. Res.*, 2013, **20**, 1596–1605.
8 C. Liu, C. Huang, C. Hu, *et al.*, *Sci. Total Environ.*, 2019, **659**, 221–229.
9 L. Yu, Z. Wang, L. Shi, *et al.*, *Appl. Catal., B*, 2012, **113**, 318–325.
10 L. Yang, Z. Li, H. Jiang, *et al.*, *Appl. Catal., B*, 2016, **183**, 75–85.
11 C. Xue, F. Zhang, Q. Chang, *et al.*, *Chem. Lett.*, 2018, **47**(6), 711–714.
12 R. Bao, J. Geng, J. Sullivan, *et al.*, *Phys. Status Solidi A*, 2018, **215**, 1800436.
13 R. Bao, C. Chen, J. Xia, *et al.*, *J. Mater. Chem. C*, 2019, **7**, 4981.
14 R. Bao, Y. Zhao, F. Ma, *et al.*, *J. Phys. Chem. Solids*, 2022, **161**, 110435.
15 X. Zhao, Y. Zhang, P. Wen, *et al.*, *Mol. Catal.*, 2018, **452**, 175–183.
16 S. Zhu and B. Yan, *New J. Chem.*, 2018, **42**, 4394–4401.

17 H. Song, Z. Sun, Y. Xu, *et al.*, *Sep. Purif. Technol.*, 2019, **228**, 115764.
18 Y. Li, C. Wang, H. Fu, *et al.*, *J. Environ. Chem. Eng.*, 2021, **9**, 105451.
19 X. Cheng, X. Dao, S. Wang, *et al.*, *ACS Catal.*, 2021, **11**, 650–658.
20 L. Wang, S. Wang, M. Li, *et al.*, *J. Alloys Compd.*, 2022, **909**, 164751.
21 S. Guo, L. Chi, T. Zhao, *et al.*, *J. Electroanal. Chem.*, 2021, **880**, 114915.
22 J. Hu, J. Ding and Q. Zhong, *J. Colloid Interface Sci.*, 2020, **560**, 857–865.
23 X. Li, Y. Pi, Q. Hou, *et al.*, *Chem. Commun.*, 2018, **54**, 1917–1920.
24 J. Wang, A. Cherevan, C. Hannecart, *et al.*, *Appl. Catal., B*, 2021, **283**, 119626.
25 Q. Huang, Y. Hu, Y. Pei, *et al.*, *Appl. Catal., B*, 2019, **259**, 118106.
26 M. Ji, L. Jin, J. Fu, *et al.*, *Environ. Chem.*, 2006, **25**, 145–148.
27 Q. Wang, J. Xu, Y. Ge, *et al.*, *Electrochim. Acta*, 2016, **198**, 165–173.
28 B. Xie and Z. Li, *Mater. Chem. Phys.*, 2006, **95**, 39–50.
29 H. Thi, K. Thi, N. Hoang, *et al.*, *Mater*, 2021, **14**(24), 7741.
30 S. Xin, S. Huo, C. Zhang, *et al.*, *Appl. Catal., B*, 2022, **305**, 121024.
31 Y. Yu, L. Piao, J. Xia, *et al.*, *Mater. Chem. Phys.*, 2016, **182**, 77–85.
32 J. Yoon, D. Kim, J. Kim, *et al.*, *Appl. Catal., B*, 2019, **244**, 511–518.
33 J. Low, J. Yu, M. Jaroniec, *et al.*, *Adv. Mater.*, 2017, **29**(20), 1601694.
34 G. Divyapriya, R. Srinivasan, J. Mohanalakshmi, *et al.*, *J. Water Process. Eng.*, 2022, **49**, 102967.
35 X. Bai, Y. Li, L. Xie, *et al.*, *Environ. Sci.: Nano*, 2019, **6**, 2850–2862.
36 X. Li, B. Wang, Y. Cao, *et al.*, *ACS Sustainable Chem. Eng.*, 2019, **7**, 4548–4563.